Chiral three-dimensional lattices with tunable Poisson's ratio

Chan Soo Ha, Michael E. Plesha, Roderic S. Lakes*

May 25, 2016

Department of Engineering Physics, University of Wisconsin, Madison, WI 53706-1687, USA
* Corresponding author. email lakes@engr.wisc.edu Phone: +00 608 265 8697

Abstract

Chiral three-dimensional cubic lattices are developed with rigid cubical nodules and analyzed via finite element analysis. The lattices exhibit geometry dependent Poisson's ratio that can be tuned to negative values. Poisson's ratio tends to zero as the cubes become further apart. The lattices exhibit stretch-twist coupling. Such coupling cannot occur in a classical elastic continuum but it can occur in a chiral Cosserat solid.

1 Introduction

Chiral materials and structures lack a center of symmetry; they are not invariant to inversion of coordinates. For example, quartz is chiral at the inter-atomic level; left and right forms exist. Chirality may also be introduced in composites on a micro, milli, or macro scale. For example, a planar chiral lattice with Poisson's ratio -1 [1] was developed to have a constant Poisson's ratio essentially independent of strain. Analysis revealed Poisson's ratio to be -1, equal to the lower limit for stability in 2D or in 3D. Experiments revealed Poisson's ratio to be approximately constant for axial compressive strains up to 25%. By contrast, negative Poisson's ratio of (3D) foams [2] and of (2D) honeycombs [3] with inverted hexagonal cells of bow-tie shape is dependent on strain. Two dimensional structures containing rotating hexamers and trimers [4] and distributions of node sizes can have negative Poisson's ratio of large magnitude. Negative Poisson's ratio materials have been called "auxetic" or "anti-rubber"; if the Poisson's ratio is independent of strain, they have been called "dilational".

Chiral 2D lattices have been studied for use as structural honeycomb [5] [6] in sandwich panels for airplane wings that morph or change shape. Buckling [7] [8] of such lattices has been studied in such a structural context. Lattices have been made with sensors and actuators for possible use as smart structures [9]. The lattices exhibit interesting characteristics in wave propagation, e.g. tunable band gaps [10].

Three dimensional lattices offer design freedom in comparison with foams [11]. For example, 3D lattices with ribs organized in a triangulated structure are stiffer than foams made of the same rib material because the ribs deform axially rather than in bending [12]. A negative Poisson's ratio 3D model was developed [13] to better understand the deformation of α-cristobalite [14], a negative Poisson's ratio form of silicon dioxide. A 3D model of cubical nodules linked at their corners

was developed [15] to model the nodule-fibril structure and properties of an auxetic microporous polymer [16]. Also, 3D lattices have been made with a negative Poisson's ratio [17]. Such lattices have been made using 3D printing methods.

If a lattice or foam contains a sufficient number of cells, it may be analyzed as a continuum. In most analyses (e.g. [11]), the continuum is a classical one; classical elasticity has no length scale. If the cell size is not negligible compared with length scales associated with the specimen or with strain gradients applied to it, then a more general continuum model may be appropriate. Cosserat (micropolar) elasticity [18] is such a continuum theory in which rotation of points has physical significance. For example, chiral lattices [1] have been analyzed [19] [20] in the context of Cosserat elasticity.

2   Analysis
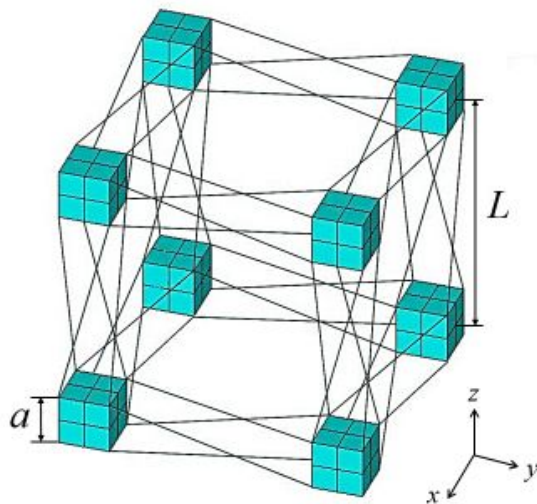
Figure 1: Unit cell of chiral lattice structure (1x1x1). The aspect ratio is defined to be L/a, where $L/a > 1$.

Lattices were constructed using the unit cell (1x1x1) shown in figure 1. This cell consists of eight rigid cubes at the corners of the cell (with edge lengths a) and multiple deformable ribs (i.e., beams) connecting various corners of cubes to one another as shown. The center-to-center cube spacing is L, and the aspect ratio for the unit cell is defined to be L/a, where $L/a > 1$. The ribs are steel with $E = 200$ GPa and $\nu = 0.3$, and circular cross section with diameter of the ribs is 10 μm. This leads to the ratio of the cube side length to the rib diameter equal to be 100.

A finite element model for the unit cell was constructed using ANSYS. Each rib was modeled using one BEAM 189 element. This beam element has three nodes with six degrees of freedom at each node (three translations and three rotations); has cubic displacement interpolations; and allows for modeling bending behavior and torsion in three dimensions. Because each rib is loaded only by forces and moments at its ends, only one BEAM 189 is needed to obtain exact (or nearly exact) response [21]. Each cube was modeled using 24 SHELL 181 elements. This shell element has four nodes with six degrees of freedom at each node (three translations and three rotations).

Bottom surface as roller-supported
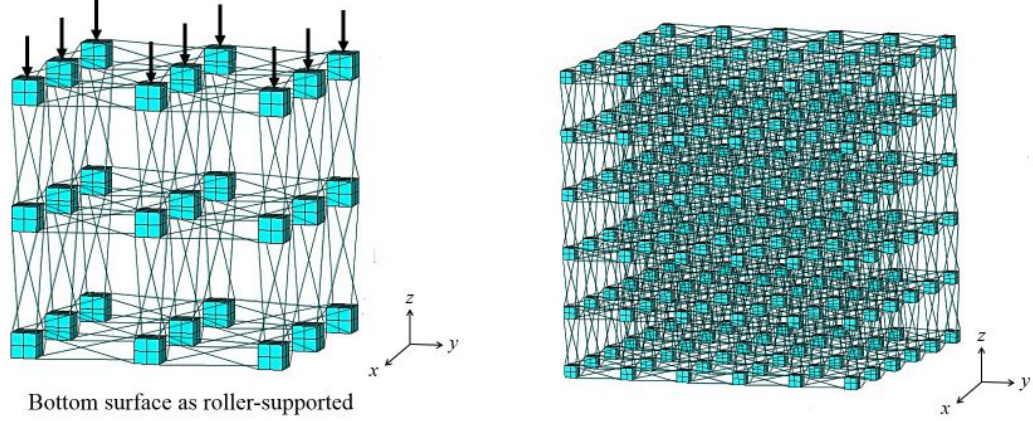
Figure 2: Examples of chiral lattice structures consisting of multiple unit cells. At left is a structure with two cells per side (2x2x2), and at right is a structure with five cells per side (5x5x5).

Its material properties were taken to be eight orders of magnitude greater than E of the ribs, so that effectively the cubes are rigid. As such, each cube is a hollow object where its six surfaces are discretized using four shell elements each. The merit of this treatment is that all nodes throughout the finite element model have the same degrees of freedom, especially rotations, which makes it straightforward to connect the ribs to the cubes. Note that it is tempting to use solid finite elements to model the cubes, but these elements have only translational degrees of freedom and hence it would be difficult to attach the ribs to the cubes since the sets of degrees of freedom for these elements are fundamentally different. Furthermore, by using four shell elements for each surface of a cube, there is a node present in the center of each cube's face, which is convenient for purposes of applying loads and supports.

Using this unit cell, lattices of multiple unit cells were constructed as shown in figure 2, and various aspect ratios including 1.5, 1.8, 2, 2.2, 5, 10 and 20 were modeled.

To determine an effective Young's modulus of the lattices in response to axial compression loading, equal point loads in the negative z direction were applied to the center node of each cube on the surface of the lattice (the surface with positive z as the normal direction) as shown in figure 2 for the 2x2x2 lattice. Support conditions on the opposite surface of the lattice (the surface with negative z as the normal direction) consisted of zero z direction translation for all center nodes on cubes, plus a small number of additional constraints to prohibit rigid body motion of the lattice. Thus, the bottom surface of the lattice is supported by rollers and the Poisson effect is allowed to fully develop.

Finite element simulations were performed for five lattice structures (1x1x1 through 5x5x5), and for seven aspect ratios for each of these. Each finite element simulation provided the displacements and rotations of all nodes in the lattice. For each unit cell in a lattice, we computed effective strains throughout the unit cell by the following process.

Using the eight x direction displacements of each cube of one unit cell, as provided by the finite element simulation, we fit the following polynomial

$$u_x = a_1 + a_2 x + a_3 y + a_4 z + a_5 xy + a_6 yz + a_7 xz + a_8 xyz \tag{1}$$

so that the coefficients $a_1 - a_8$ could be determined. Similarly, this process was repeated to obtain polynomials for the y and z direction displacements, namely u_y and u_z. Equation 1 allows one to

3

embody the notion of average strain in a continuum model. Then, using the standard definition of small strains

$$\epsilon_{ij} = \frac{1}{2}(\frac{\partial u_i}{\partial x_j} + \frac{\partial u_j}{\partial x_i}) \tag{2}$$

where x_1, x_2 and x_3 correspond to x, y and z, respectively, we determine the effective strains throughout each unit cell of a lattice. Note that this entire process is identical to using the shape functions and $[B]$ matrix for an 8-node brick finite element. Thus, by using the $[B]$ matrix given in [21], along with the displacements of each cube in the unit cell, the effective strains throughout each unit cell are easily determined by evaluating $\{\epsilon\} = [B]\{d\}$.

3 Results and discussion
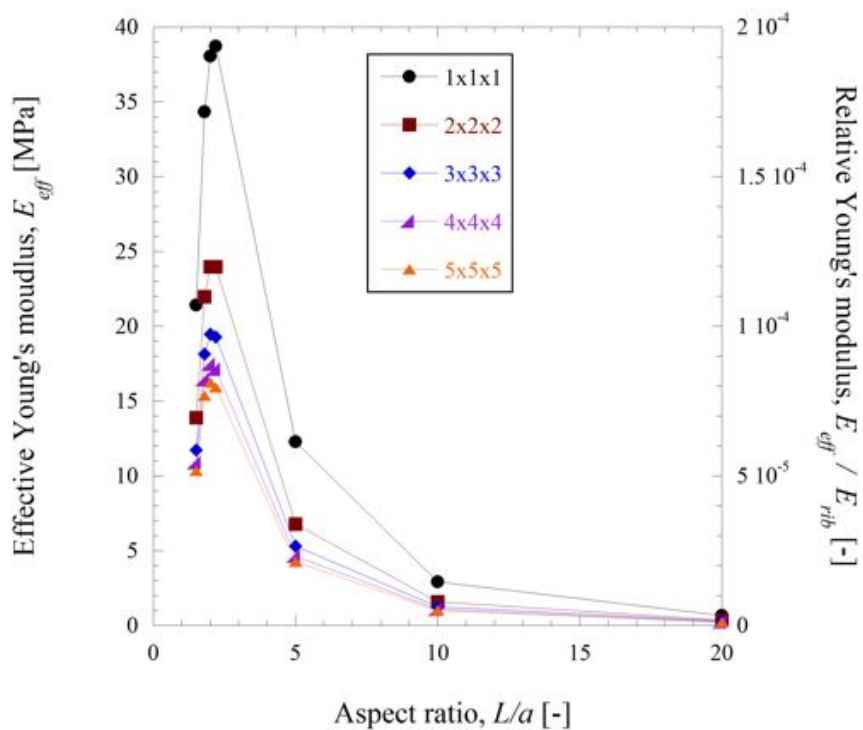
Figure 3: Effective Young's modulus in a principal direction vs. aspect ratio for chiral lattice.

4
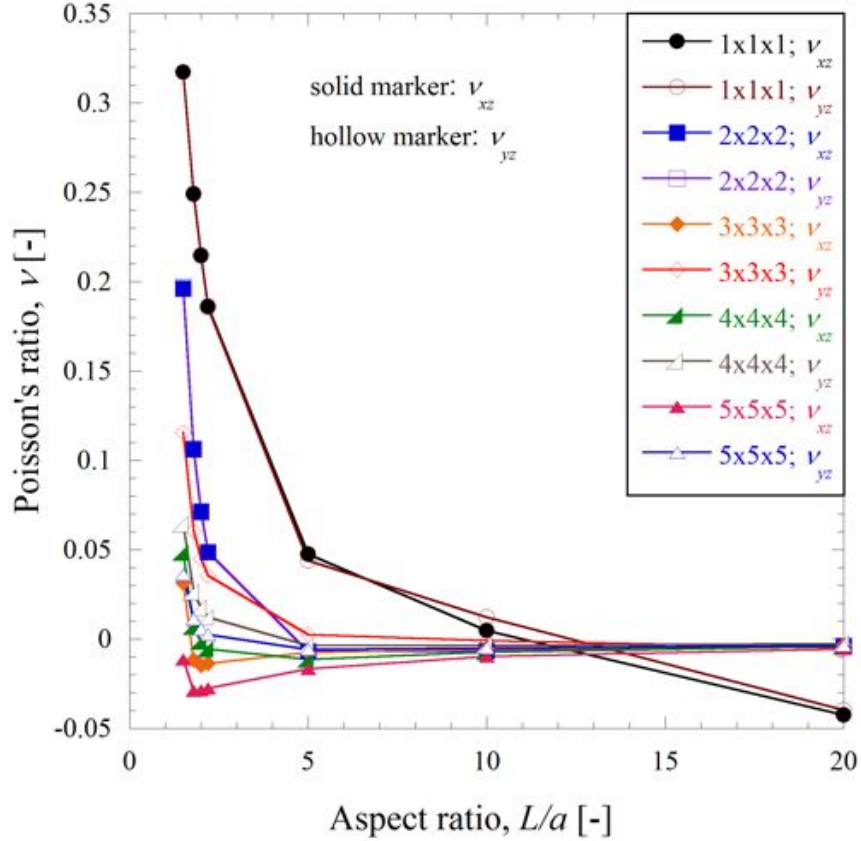
Figure 4: Poisson's ratio in a principal direction vs. aspect ratio for chiral lattice.

The effective Young's modulus in a principal direction versus aspect ratio for chiral lattice is shown in figure 3. The relative Young's modulus, E_{eff}/E_{rib}, was also plotted in this figure. The effective Young's modulus first rises then decreases with aspect ratio. The decrease occurs because the round section rib elements are of constant diameter, but their length increases with aspect ratio. The lower modulus for the smallest aspect ratio is a result of the highly oblique angle of the ribs with respect to the nodules.

Poisson's ratio of the chiral lattice depends on the aspect ratio, as shown in figure 4. Poisson's ratio in a principal direction tends to zero as relative rib slenderness increases except when there is only one cell. Poisson's ratio can be negative provided there are a sufficient number of cells, and for an appropriate range of aspect ratio near 2. The minimum in Poisson's ratio was delineated by conducting studies at fine intervals of Poisson's ratio. As the number of cells is increased, the lattice can be envisaged to approach a continuum for which continuum concepts are appropriate. The model with only one cell is better viewed as a structure; it is included in the plot for completeness.

Lattices exhibit stretch twist coupling, as shown in figure 5. Coupling increases with the aspect ratio except for a single cell; coupling decreases slowly with the number of cells.
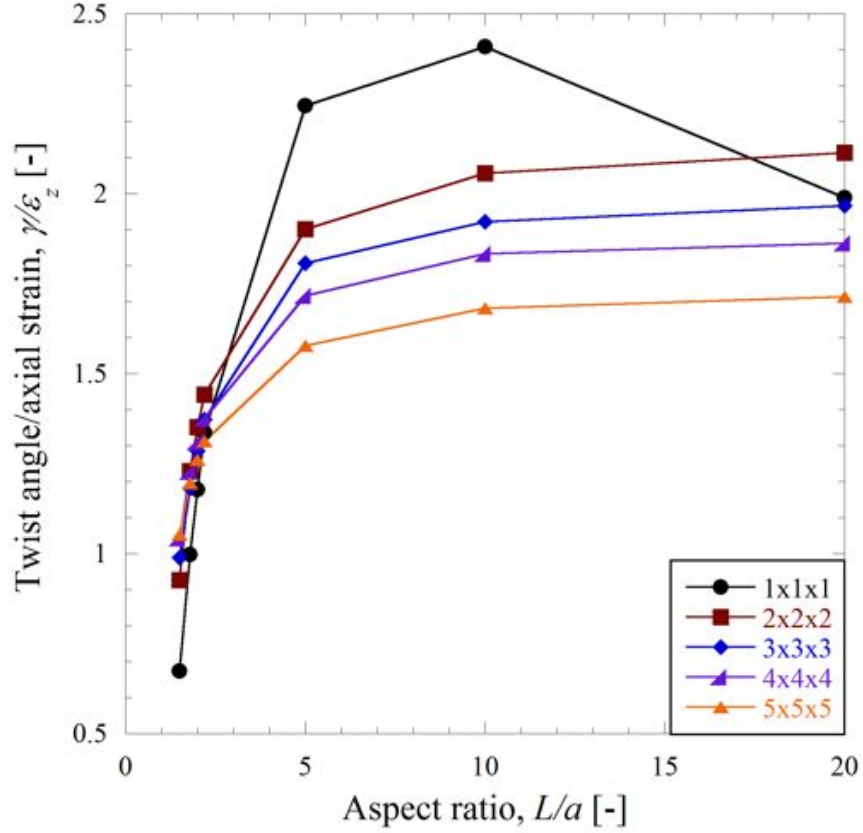
Figure 5: Stretch twist coupling, ratio of torsion strain / axial strain vs. aspect ratio for chiral lattice.

As the number of cells increases, the effective Young's modulus appears to converge to a constant value as shown in figure 6. Convergence of the Poisson's ratio to an asymptotic constant value is slower. The Poisson's ratios for orthogonal directions are unequal: $\nu_{xy} \neq \nu_{yx}$. Lattices with an even number of cells on a side exhibit less anisotropy than those with an odd number of cells on a side. For a cubic classical elastic continuum, these Poisson's ratios are equal. More cells would be needed to probe convergence of Poisson's ratio to the constant, symmetric value of a classical continuum.
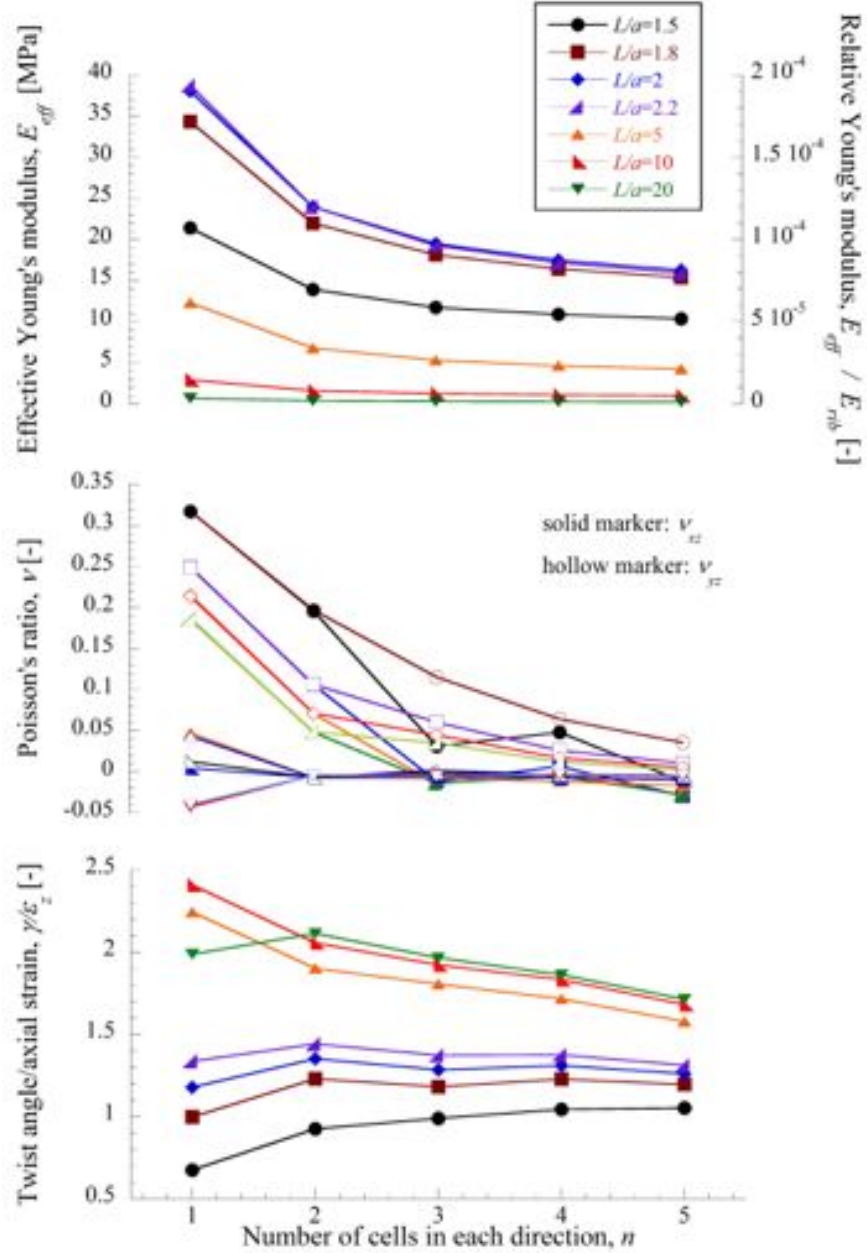
Figure 6: Effective Young's modulus, Poisson's ratio and stretch twist coupling vs. number of cells on a side.

Stretch twist coupling in the limit of a classical elastic continuum must be zero but in this series, no such asymptotic limit is reached. In the limit of sufficiently many cells, the lattice is expected to be treatable as an equivalent continuum as is done with foams [11]. However, the continuum need not be classical. Use of a non-classical continuum model can account for some of the response of the chiral lattice as follows.

Stretch-twist coupling is associated with chirality. The twisting is either to the left or to the right. The material or structure must have the requisite asymmetry, specifically chirality, to exhibit such behavior. As for continuum models, classical elasticity does not distinguish left from right. The reason is that classical elasticity is a fourth rank tensor property. An inversion of all coordinate axes

converts left to right but has no effect on tensor properties of even rank. Therefore more freedom is needed in a continuum model to account for chiral elastic effects. Cosserat elasticity provides sufficient freedom. Cosserat solids incorporate rotational degrees of freedom in the microstructure in addition to the usual translation. Cosserat solids exhibit a characteristic length scale in contrast to classically elastic solids. There are six elastic constants for a 3D isotropic, non-chiral Cosserat solid; nine constants for a 3D chiral solid. Cosserat elastic constants were calculated by analysis [19] of 2D chiral lattices [1] and determined experimentally in non-chiral foams [22] [23].

For 3D chiral solids viewed as a continuum, chiral Cosserat constitutive equations [24] are considered.

$$\sigma_{kl} = \lambda \epsilon_{rr} \delta_{kl} + 2G\epsilon_{kl} + \kappa e_{klm}(r_m - \phi_m) + C_1 \phi_{r,r} \delta_{kl} + C_2 \phi_{k,l} + C_3 \phi_{l,k} \tag{3}$$

$$m_{kl} = \alpha \phi_{r,r} \delta_{kl} + \beta \phi_{k,l} + \gamma \phi_{l,k} + C_1 \epsilon_{rr} \delta_{kl} + (C_2 + C_3)\epsilon_{kl} + (C_3 - C_2)e_{klm}(r_m - \phi_m) \tag{4}$$

The elastic constants C_1, C_2 and C_3 represent the effect of chirality. There are nine elastic constants compared with six for isotropic non-chiral Cosserat elasticity, and two for classical elasticity. As with the non-chiral case, characteristic lengths are defined based on ratios of tensorial constants; further detail is provided in an experimental study of non-chiral foam [22]. The chiral isotropic Cosserat model predicts the following.

(1) Stretch-twist coupling in a round rod of isotropic chiral material occurs and is a function of all nine elastic constants [24].

(2) Stretch-twist coupling in a round rod is nearly constant for small rod radius R; $\gamma/\epsilon \sim 1/R$ for large R much larger than the characteristic length.

(3) The transverse deformation associated with the Poisson effect is nonuniform though the material is assumed to be a uniform continuum.

The present chiral lattice has cubic symmetry and the shape is cubic, so a direct correspondence with isotropic continuum models is not to be expected. Nevertheless, the stretch twist coupling exhibited by the lattice and its slow decrease with size is anticipated in the continuum view. More detail on the Cosserat interpretation is to be provided elsewhere. The lattice model may also be modified to obtain orthotropic symmetry by providing different spacing of nodules in three orthogonal directions.

Poisson's ratio of individual cells vs. cell position in two transverse directions is shown in figure 7 and figure 8. As anticipated via the Cosserat continuum view, the Poisson effect is not homogeneous; it depends on position. The Poisson's ratio reported for the lattice as a whole, figure 4, refers to the Poisson's ratio based on changes in the outer dimensions, corresponding to standard measurement methods. The lattice, which is cubic not isotropic, exhibits anisotropy in the Poisson effect.
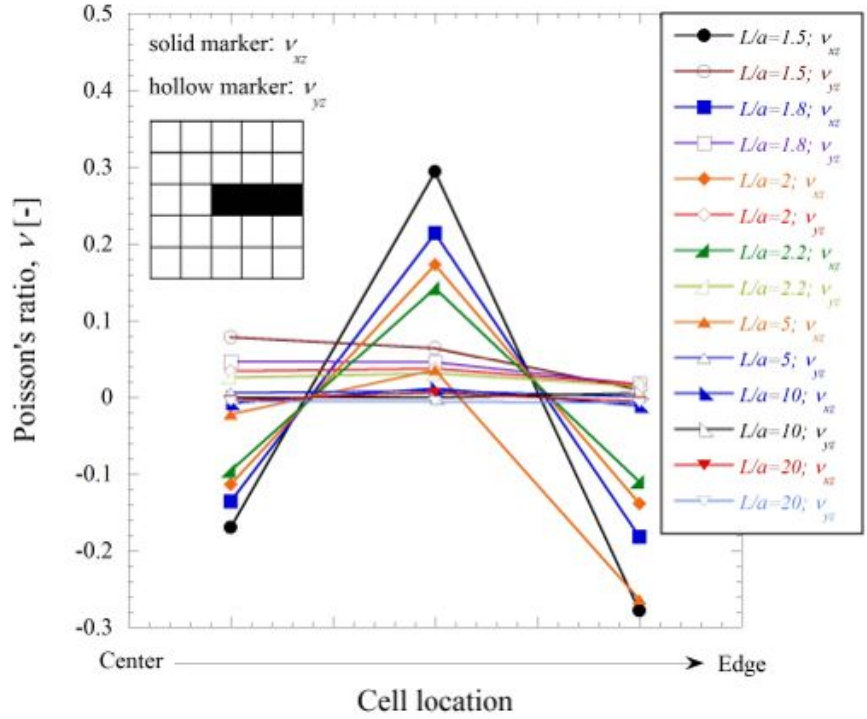
Figure 7: Poisson's ratio of individual cells vs. cell position in x direction for chiral 5x5x5 lattice.
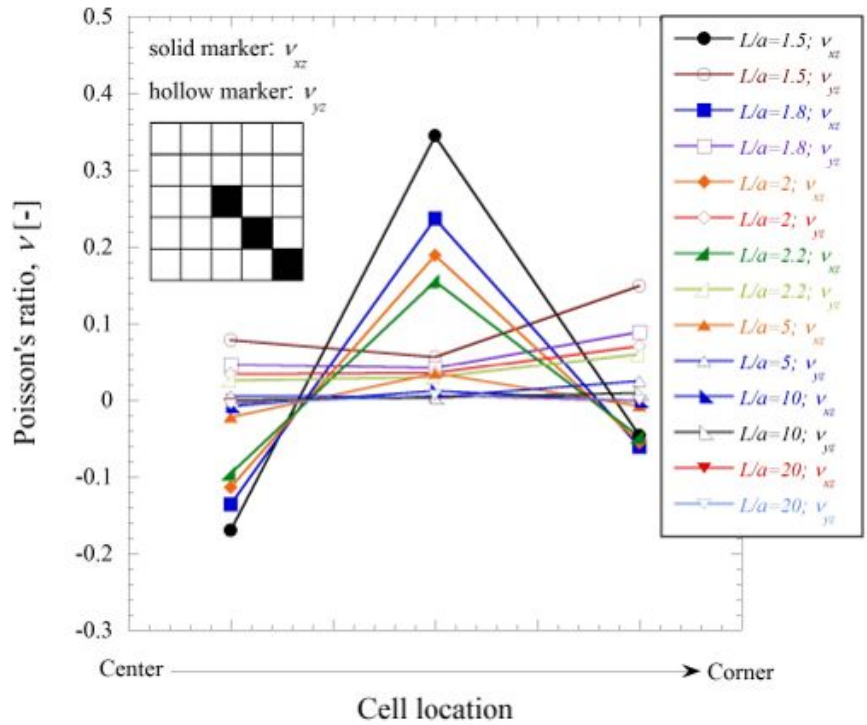
Figure 8: Poisson's ratio of individual cells vs. cell position in diagonal transverse direction for chiral 5x5x5 lattice.

The ribs in the present lattice were assumed to be made of a single material. Lattices with bi-material ribs have been studied in the context of control of thermal expansion or of piezoelectric sensitivity. For example, 2D lattices have been formulated and analyzed with controllable positive or negative expansion of large or small magnitude [25] [26], or zero thermal expansion [26] [29]. Also, 2D lattices with bi-material piezoelectric elements [27] were studied experimentally [28]; these lattices exhibit large values of piezoelectric sensitivity.

4   Conclusion

Chiral 3D lattices exhibit stretch-twist coupling that increases with relative slenderness of ribs. Poisson's ratio depends on geometry and can be negative. Chiral 3D lattices also exhibit Poisson's ratio that tends to zero as relative rib slenderness increases. The lattices have cubic structure and cubic symmetry. Isotropic solids are conceptually easier to model, therefore future development of lattices can aim to achieve material isotropy of the equivalent continuum.

References

[1] D. Prall and R. S. Lakes, Properties of a chiral honeycomb with a Poisson's ratio -1, Int. J. of Mechanical Sciences, **39**, 305-314, (1996).

[2] R. S. Lakes, Foam structures with a negative Poisson's ratio, Science, **235** 1038-1040 (1987).

[3] L. J. Gibson, M. F. Ashby, G. S. Schajer, and C. I. Robertson, The mechanics of two dimensional cellular solids, Proc. Royal Society London, **A382**, 25-42 (1982).

[4] A. A. Pozniak and K. W. Wojciechowski, Poisson's ratio of rectangular anti-chiral structures with size dispersion of circular nodes, Phys. Stat. Sol. (b) **251**, 367-374, (2014).

[5] D. Bornengo, F. Scarpa, C. Remillat, Evaluation of hexagonal chiral structure for morphing airfoil concept, Proceedings of the Institution of Mechanical Engineers, Part G: Journal of Aerospace Engineering **219** 185-192 (2005).

[6] J. Martin, J. Heyder-Bruckner, C. Remillat, F. Scarpa, K. Potter, M. Ruzzene, The hexachiral prismatic wingbox concept, Phys. Stat. Sol. (b) **245** 570-571 (2008).

[7] A. Spadoni, M. Ruzzene and F. Scarpa, Global and local linear buckling behavior of a chiral cellular structure, Phys. Stat. Sol. (b) **242** 695-709 (2005).

[8] W. Miller, C.W. Smith, F. Scarpa, K.E. Evans, Flatwise buckling optimization of hexachiral and tetrachiral honeycombs, Composites Science and Technology, **70**, 1049-1056, (2010).

[9] H. Abramovitch, M. Burgard, L. Edery-Azulay, K.E. Evans, M. Hoffmeister, W. Miller, F. Scarpa, C.W. Smith, K.F. Tee, Smart tetrachiral and hexachiral honeycomb: Sensing and impact detection, Composites Science and Technology **70**, 1072-1079 (2010).

[10] A. Spadoni, M. Ruzzene, S. Gonelli, F. Scarpa, Phononic properties of hexagonal chiral lattices, Wave Motion **46** (7), 435-450 (2009).

[11] L. J. Gibson, and M. F. Ashby, *Cellular Solids*, Pergamon, Oxford, 1988; 2nd Ed., Cambridge, (1997).

[12] A. J. Jacobsen, W. Barvosa-Carter, S. Nutt, Compression behavior of micro-scale truss structures formed from self-propagating polymer waveguides, Acta Materialia, **55**, 6724-6733, 2007.

[13] Alderson A, Evans KE (2001) Rotation and dilation deformation mechanisms for auxetic behavior in the α-cristobalite tetrahedral framework structure. Physics and Chemistry of Minerals 28(10):711-718.

[14] Haeri, A. Y., Weidner, D. J., and Parise, J. B., Elasticity of alpha-cristobalite: a silicon dioxide with a negative Poisson's ratio, Science, 257, 650-652 (1992).

[15] Gaspar N, Smith CW, Alderson A, Grima JN, Evans KE (2011) A generalised three-dimensional tethered-nodule model for auxetic materials. Journal of Materials Science 46(2):372-384.

[16] Alderson KL, Webber RS, Evans KE (2007). Microstructural evolution in the processing of auxetic microporous polymers. Phys Status Solidi B 244(3):828-841.

[17] T. Buckmann, R Schittny, M Thiel, M Kadic, GW Milton and M Wegener, On three-dimensional dilational elastic metamaterials, New Journal of Physics **16** 033032 (2014).

[18] A.C. Eringen, Theory of micropolar elasticity. In Fracture Vol. **1**, 621-729 (edited by H. Liebowitz), Academic Press (1968).

[19] X. N. Liu, G. L. Huang, G. K. Hu, Chiral effect in plane isotropic micropolar elasticity and its application to chiral lattices, J. of the Mechanics and Physics of Solids **60**, 1907-1921 (2012).

[20] A. Spadoni, M. Ruzzene, Elasto-static micropolar behavior of a chiral auxetic lattice, J. of the Mechanics and Physics of Solids **60**, 156-171 (2012).

[21] Cook, R.D., Malkus, D.S., Plesha, M.E., and Witt, R.J., Concepts and Applications of Finite Element Analysis, 4th edition, John Wiley and Sons publishers, (2002).

[22] R. S. Lakes, Experimental microelasticity of two porous solids, Int. J. Solids and Structures, **22** 55-63 (1986).

[23] W. B. Anderson and R. S. Lakes, Size effects due to Cosserat elasticity and surface damage in closed-cell polymethacrylimide foam, Journal of Materials Science, **29**, 6413-6419, (1994).

[24] R. S. Lakes and R. L. Benedict, Noncentrosymmetry in micropolar elasticity, International Journal of Engineering Science, **29** (10), 1161-1167, (1982).

[25] R. S. Lakes, Cellular solid structures with unbounded thermal expansion, J. of Materials Science Letters, **15**, 475-477 (1996).

[26] R. S. Lakes, Solids with tunable positive or negative thermal expansion of unbounded magnitude, Applied Phys. Lett. **90**, 221905 (2007).

[27] R. S. Lakes, Piezoelectric composite lattices with high sensitivity, Philosophical Magazine Letters **94**, (1), 37-44 (2014).

[28] B. Rodriguez, H. Kalathur, and R. S. Lakes, A sensitive piezoelectric composite lattice: experiment, Phys. Stat. Sol. (b) **251**(2) 349-353 (2014).

[29] J. J. Lehman, and R. S. Lakes, Stiff, strong zero thermal expansion lattices via the Poisson effect, Journal of Materials Research, **29**, 2499-2508, (2013).